Catal Lett (2008) 126:164–172
DOI 10.1007/s10562-008-9599-x

Sol–Gel Assisted Preparation of Chromia–Silica Catalysts for Non-Oxidative Dehydrogenation of Propane

Igor Martyanov · Abdelhamid Sayari

Received: 6 May 2008 / Accepted: 21 July 2008 / Published online: 9 September 2008

Abstract Preparation of continuous silica gel in the presence of dissolved $Cr(NO_3)_3$ leads to a hard high surface area (710 m^2/g) microporous xerogel. Formation of the gel in the pore structure of mesoporous Pore-Expanded MCM-41 (PE-MCM-41) and macroporous commercial Cab–O–Sil silica results in retention of the mesoporous structure in the case of PE-MCM-41, and the formation of a powder with a broad pore size distribution in the case of Cab–O–Sil silica. Comparison of the catalytic activities in non-oxidative dehydrogenation of propane revealed a linear correlation of the initial conversion with the surface area for all three samples. The sample prepared from PE-MCM-41 through a sol–gel assisted procedure was the most active, particularly with respect to the catalysts prepared by simple wet impregnation with chromium nitrate.

Keywords Propane · Propylene · Dehydrogenation · MCM-41 · Chromium · Catalyst

1 Introduction

Catalysts based on chromia have received much attention due to their favorable properties in various important processes. Examples are numerous and include catalytic oxidation of organic compounds [1–3], large-scale polymerization of ethylene into polyethylene over Phillips CrO_x/SiO_2 catalysts [4], potential use of chromia supported catalysts in the processes of chlorinated carbon removal [5], and others. Non-oxidative dehydrogenation over CrO_x/Al_2O_3 catalysts is an important industrial process for producing propylene from propane [6, 7]. As demand for propylene and the price difference between propane and propylene are rising [8], it is expected that more propylene would be produced this way.

Widespread application of chromia supported catalysts and the rich chemistry of chromium compounds laid ground for a steady interest towards the structure of supported chromium oxides, the nature of active sites and the mechanisms of the catalytic reactions [6, 7, 9, 10]. However, despite extensive studies of non-oxidative dehydrogenation processes, the oxidation state of active chromium species remains under debate with some early studies favoring Cr^{2+} species [11] and more recent work advocating the importance of Cr^{3+} sites [12–15] or both [16, 17].

There are quite a few approaches to prepare chromia-based catalysts for non-oxidative dehydrogenation processes including impregnation, coprecipitation and atomic layer epitaxy. The need to achieve high dispersion dictates the necessity of anchoring chromia species onto the surface of the support. In the most thoroughly studied method, i.e., incipient wetness impregnation with aqueous solution of chromium(VI) oxide, the anchoring occurs upon heating through esterification-like reaction of chromates with surface hydroxyl groups [9]. Sol–gel preparation affords high surface area silica, alumina and other oxides. Carried out in the presence of dissolved transition metal salts, such an approach can lead to large surface area materials with metal ions in a highly dispersed state.

In recent years, considerable attention has been paid to a new class of materials—mesoporous molecular sieves. Apart from having very high surface areas, they possess narrow pore size distributions and ordered pore structure [18]. The pore size of these materials can be controlled

I. Martyanov · A. Sayari (✉)
Department of Chemistry, University of Ottawa, Ottawa, ON, Canada K1N 6N5
e-mail: abdel.sayari@uottawa.ca

within a broad range by using strategies including post-synthesis hydrothermal treatment of uncalcined mesoporous silica in the presence of pore expanding agents as was discovered by Sayari and co-workers [19–21]. The use of mesoporous molecular sieves combined with the formation of chromia-doped gel inside their pores may give rise to catalysts with unusual properties as the porous structure can be independently manipulated, whereas the sol–gel step would favor high chromia dispersion.

In this paper, we describe preliminary results on sol–gel assisted preparation of chromia/silica catalysts in the presence of preformed silica powder: Pore Expanded MCM-41 (PE-MCM-41) and commercial Cab–O–Sil M-5 silica. The results are compared to chromia–silica samples prepared in the absence of preformed silica powders, and with chromia–silica samples prepared via impregnation of PE-MCM-41 and Cab–O–Sil M-5 silica with chromium salts. The prepared catalysts were tested in the reaction of non-oxidative dehydrogenation of propane.

2 Experimental

Chromium nitrate ($Cr(NO_3)_3 \cdot 9H_2O$), tetraethyl orthosilicate (TEOS, $Si(OEt)_4$) from Aldrich, isopropanol (^{i}PrOH) from Fisher, powdered commercial Cab–O–Sil M-5 silica (Cab–O–Sil) from Cabot Corp. were used as received. Distilled water was used when required. PE-MCM-41 was prepared in house according to a procedure described elsewhere [22].

Five chromia–silica catalysts were synthesized, characterized and tested in non-oxidative dehydrogenation reaction. They were CrO_x/SiO_2xr/PE-MCM-41 and CrO_x/SiO_2xr/Cab–O–Sil prepared by depositing a silica–chromia gel in within the pore structure of PE-MCM-41 and Cab–O–Sil silica; CrO_x/SiO_2xr prepared by the sol–gel method, and CrO_x/PE-MCM-41 and CrO_x/Cab–O–Sil prepared by impregnation. Two key steps were considered in the design of the catalyst synthesis procedure. First, the appropriate relative amounts of TEOS, water, and isopropanol were determined to ensure the formation of silica gel in the presence of various concentrations of the chromium salt in a reasonable time period. Second, an amount of the liquid mixture to be added to a pre-weighted amount of PE-MCM-41 was measured to make a thick paste. This second step aimed at filling the pores of PE-MCM-41, while minimizing the amount of liquid in the interparticle space, thus minimizing future formation of gel outside of PE-MCM-41 pores. As the relative amounts of TEOS, water and isopropanol in the preparation of CrO_x/SiO_2xr/PE-MCM-41 were held the same as for chromium-doped xerogel, CrO_x/SiO_2xr, to ensure gelation, the concentration of chromium was adjusted to produce the same Cr/Si = 0.45 mol% final ratio as for CrO_x/SiO_2xr. A similar procedure was adopted to prepare chromium-doped xerogel coated Cab–O–Sil silica sample, CrO_x/SiO_2xr/Cab–O–Sil. In the preparation of CrO_x/PE-MCM-41 and CrO_x/Cab–O–Sil samples, TEOS was substituted by a similar volume of isopropanol with amounts of chromium salt adjusted to yield Cr/Si = 0.45 mol% ratios.

The synthesis of chromia-doped xerogel, CrO_x/SiO_2xr, was carried out as follows. A mixture of TEOS, water and isopropanol taken in volume proportions of 40/28/135 and containing a pre-determined amount of $Cr(NO_3)_3 \cdot 9H_2O$ was prepared. The mixture was left to gel overnight at 70 °C followed by the gel drying at the same temperature. The calcination step was carried out under flowing air with the furnace temperature rising from room temperature to 600 °C at 10 °C/min, holding at 600 °C for 4 h followed by cooling to room temperature.

CrO_x/SiO_2xr/PE-MCM-41 was prepared as follows. First a solution of the required amount of $Cr(NO_3)_3 \cdot 9H_2O$ in TEOS/H_2O/^{i}PrOH = 40/28/135 mL/mL/mL was prepared. About 15 mL of this solution was gradually added while mixing with a spatula to 2.7 g of pre-calcined PE-MCM-41. The obtained thick paste was aged at 70 °C to achieve gelation inside the pores, dried then calcined in a similar way as the CrO_x/SiO_2xr sample.

The preparation of CrO_x/SiO_2xr/Cab–O–Sil was analogous to CrO_x/SiO_2xr/PE-MCM-41. It involved addition of 20 mL of the solution of chromium nitrate in TEOS/H_2O/^{i}PrOH = 40/28/135 by volume to 3.48 g of SiO_2 Cab–O–Sil M-5. The gelation, drying and calcination steps were as described for CrO_x/SiO_2xr.

CrO_x/PE-MCM-41 powder was prepared by addition of 15 mL of the solution of $Cr(NO_3)_3 \cdot H_2O$ in H_2O/^{i}PrOH = 28/175 mL/mL to 2.7 g of pre-calcined PE-MCM-41. Aging at 70 °C, drying and calcination steps were identical to those used for other samples.

CrO_x/Cab–O–Sil catalyst was prepared through mixing of 20 mL of $Cr(NO_3)_3 \cdot H_2O$ in H_2O/^{i}PrOH = 28/175 mL/mL with 3.48 g of Cab–O–Sil, followed by aging at 70 °C, drying and temperature programmed calcination up to 600 °C in air.

The molar ratios of Cr/Si/Si in CrO_x/SiO_2xr/PE-MCM-41 and in CrO_x/SiO_2xr/Cab–O–Sil samples as derived from the preparation recipe were approximately 2/100/340 and 1.9/100/330 mol% respectively. The molar ratios of chromium to total silicon were the same for all catalysts, ca. 0.45 mol%.

Raman spectra (200–1200 cm^{-1}, ca. 4 cm^{-1} resolution) were recorded with a HORIBA Jobin Yvon Lab-Ram-IR HR800 Confocal Microscope. Pelletization with a press was found to substantially improve signal to noise ratio and was used with all powder samples subjected to analysis. To exclude noticeable background signal from the supporting

glass slide, a gold-coated glass slide was used instead. Collection of Raman spectra was carried out via irradiation of the sample pellets with the focused beam of an Ar^+ laser (514.5 nm). The scattered light was collected by 100× lens having 0.9 numerical aperture. The accumulated Raman spectra were an average of 20 scans with 10 s per scan per spectral region.

Diffuse reflectance UV–Vis spectra (250–800 nm, 5 nm resolution) of the powdered samples were recorded on a Cary 300 UV–Vis spectrometer equipped with a diffuse reflectance accessory. Each spectrum was the result of a single scan with PTFE powder taken as a reference.

Temperature Programmed Reduction (TPR) experiments were carried out on AMI-200 from Altamira Instruments. In a typical procedure, the catalysts were initially calcined in a stream of 5% oxygen in helium, 30 mL/min, by ramping the temperature at 10 min^{-1} from 40 °C to 600 °C and back to 40 °C. Flushing with argon was followed by TPR of the in-situ calcined catalysts in 30 mL/min flow of 10% hydrogen in helium with the temperature increasing from 40 °C to 600 °C at 10 min^{-1}. Consumption of hydrogen was recorded by a TCD detector, which was calibrated after each experiment via pulse injection of 57 μL of 10% hydrogen in helium mixture. The H/Cr molar ratios were determined from the amount of H_2 consumed to the total amount of chromium in the samples.

Specific surface areas (BET model) and pore size distributions (BJH model with the Kruk-Jaroniec-Sayari correction [23]) of the samples were derived from the corresponding nitrogen adsorption isotherms measured with ASAP 2020 Surface Porosity Analyzer from Micromeritics. Before the measurements, the samples were degassed at 200 °C until the residual pressure of $5 \cdot 10^{-6}$ torr. Since a typical granulation procedure of as-prepared catalyst powders involved pelletization with a press and was found to affect the pore size distributions, all measurements were carried out with granulated catalysts.

Kinetic studies of propane dehydrogenation were carried out in a flow reactor at atmospheric pressure. An in-house built experimental setup included 3 mass flowmeters, four 2-way pneumatic valves, furnace with a temperature controller, and a software with the ability to set gaseous flows, operate valves and take readings. All lines after the reactor and a parallel by-pass (1/4 inch tube) were heated at 150 °C to avoid condensation of heavy products. Temperature readings were taken at a number of locations including the catalyst bed. Under steady-state conditions, a deviation in thermocouples' readings usually did not exceed ±2 °C.

A typical testing procedure consisted of several steps. First, the calcined powdered catalysts were granulated via pelletization with a press at 4000 psi followed by crushing with mortar and pestle and sieving. About 1 g of 250 μm < d < 425 μm fraction of catalyst was placed on quartz wool into a 1/2 inch stainless steel reactor equipped with welded-in stainless steel mesh. Placing quartz wool on the top of the catalyst bed and connecting the reactor to the experimental setup completed the reactor assembling. The catalyst bed was flushed with He at room temperature followed by He flow redirection to the by-pass. The temperature of the reactor was raised to 600 °C, and pre-calibrated flows of gases were set to deliver 10 mol% of propane in helium with 100 mL/min total flow. The gas feed was analyzed on-line by gas chromatography every 10 min. After stabilization of propane concentration, the flow was directed through the reactor. The first points on conversion kinetic curves were taken 5 min after the reaction mixture began to pass over the catalyst.

A gas chromatograph CP-3800 from Varian equipped with 6-way injection valve was employed for on-line analysis of the reactor effluents. Organic gaseous compounds were separated at 180 °C on a GS-GasPro column (60 m × 0.34 mm ID) from J&W Scientific and analyzed by an FID detector. The propane conversion and selectivity towards propylene were calculated as follows:

$$\text{Conversion} = \left(1 - \frac{[\text{Propane}]}{[\text{Propane}]_0}\right) \cdot 100\%,$$

$$\text{Selectivity} = \frac{[\text{Propylene}]}{[\text{Propane}]_0 - [\text{Propane}]} \cdot 100\%,$$

where $[\text{Propane}]_0$ and [Propane] are the concentrations of propane at inlet and outlet of the reactor, and [Propylene] is the concentration of propylene at the reactor's outlet. The calculations were carried out on the basis of the areas under corresponding peaks of chromatograms with relative sensitivities of FID detector reported in [24].

3 Results and Discussion

The Raman spectra of calcined catalysts before their use in the catalytic reaction are shown in Fig. 1. Though the low intensity of chromia signal and the considerable contribution from the silica support complicated a detailed analysis, some important Raman bands were clearly detected. The Raman band at 898 cm^{-1} was observed for all the samples whose preparation involved a sol–gel step: CrO_x/SiO_2xr/PE-MCM-41, CrO_x/SiO_2xr, CrO_x/SiO_2xr/Cab–O–Sil. An intense Raman band at 551 cm^{-1} with less pronounced bands at 308, 350 and 609 cm^{-1} were observed for CrO_x/Cab–O–Sil sample, whereas the bands at 554 and 898 cm^{-1} were characteristic of CrO_x/PE-MCM-41.

UV–Vis spectroscopy provided valuable additional information in regard to the degree of dispersion of

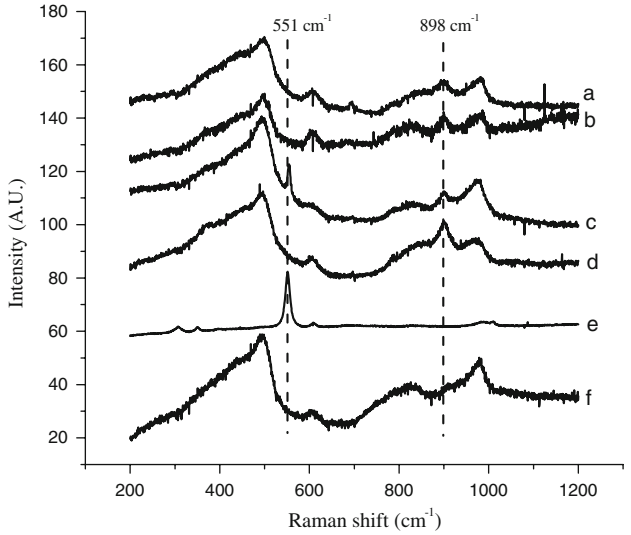

Fig. 1 Ambient Raman spectra of CrO_x/SiO_2 xr/PE-MCM-41 **a**, CrO_x/SiO_2 xr **b**, CrO_x/PE-MCM-41 **c**, CrO_x/SiO_2 xr/Cab–O–Sil **d**, CrO_x/Cab–O–Sil **e**, PE-MCM-41 **f**

supported chromia species. Typical UV–Vis spectra of some calcined catalysts are shown in Fig. 2. UV–Vis spectra of all the three catalysts, CrO_x/SiO_2xr/PE-MCM-41, CrO_x/SiO_2xr and CrO_x/SiO_2xr/Cab–O–Sil, were qualitatively similar with bands/shoulders at 276, 348, 442 nm being clearly observed.

The structure of chromia on various supports has been intensively studied in the past. Despite considerable efforts, interpretation of experimental results often remains a complex issue. In order to interpret our Raman and UV–Vis data, it would be useful to briefly summarize the main literature results obtained using these spectroscopies.

Deo and Wachs [25] developed an interesting approach to predicting the structure of various metal oxides on

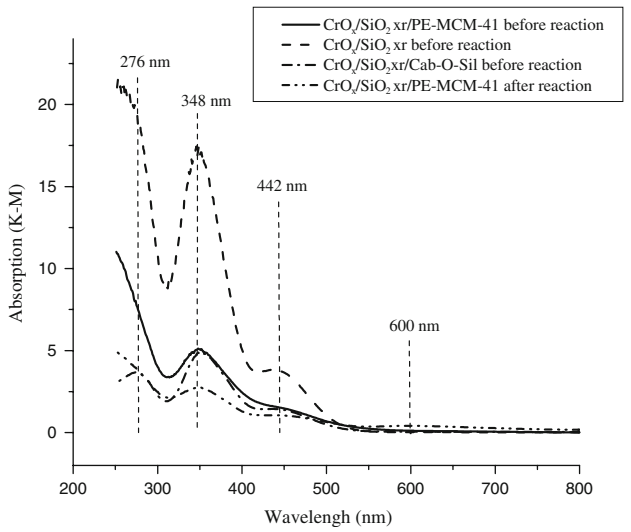

Fig. 2 Ambient UV–Vis spectra of some catalysts before and after reaction

different support materials. According to their hypothesis, under ambient conditions, the surface of oxide support is hydrated and transition metal oxides are in essence in an aqueous medium. Since the degree of polymerization of transition metal oxides strongly depends on pH of the solution, in application to supported oxides it translates into dependence on the isoelectric point, IEP, (pH at zero surface charge) of the supporting oxides. It is well known that chromate, CrO_4^{2-}, stable in basic solutions, pH > 8, would form dichromate, $Cr_2O_7^{2-}$, for pH in the range 2–6 [9]. Accordingly, on alumina with IEP close to 8.9, formation of chromates is expected, whereas on silica with IEP around 2–4, formation of dichromate with some chromate is likely.

Raman spectra of chromia species on alumina and silica supports were studied earlier [3, 26–29]. The interpretation was largely based on the comparison with the Raman spectra obtained for aqueous solutions of chromate and dichromate species [28]. In particular, chromate ions, CrO_4^{2-}, in tetrahedral environment exhibited strong band at 848 cm^{-1} (symmetrical stretching mode) with a weaker shoulder at 886 cm^{-1} (antisymmetrical stretching mode). For dichromate ions, $Cr_2O_7^{2-}$, vibrations were shifted to higher wavenumbers, with a strong band at 904 cm^{-1} and a shoulder at 942 cm^{-1}. Further increase in pH led to the formation of trichromate with Raman bands at 962, 904 and 846 cm^{-1}. Similar results were obtained by Hardcastle and Wachs [29].

Weckhuysen et al. [30] studied Raman spectra of chromia–silica and chromia–alumina samples under ambient conditions as a function of chromia loading. For hydrated chromia/alumina samples, an increase in loading of chromia from 0.2 wt to 8 wt% Cr was accompanied by a shift in the position of the single band from 865 to 900 cm^{-1} with simultaneous appearance of shoulders on both sides. The considerable 35 cm^{-1} shift was attributed to the change of chromia structure from mono- to di- and polychromates. As for chromia–silica samples, increase in chromia loading led to evolution of a single band at 895 cm^{-1} for 0.2 wt% Cr into a triplet with bands at 850, 900, and 950 cm^{-1} for 8 wt% Cr. Rather small shift in the position of the band from 895 cm^{-1} to 900 cm^{-1} (for the central band) suggests the formation of dichromate even at very low chromium loading (0.2 wt% Cr) and their conversion into polychromates as chromium loading goes up.

Important information can also be obtained from UV–Vis spectra of the supported chromia samples. Weckhuysen et al. [31, 32] used UV–Vis spectra of known compounds, i.e. K_2CrO_4, $K_2Cr_2O_7$, $Cr(NO_3)_3 \cdot 9H_2O$, for detailed analysis of chromia on silica and alumina supports. For silica–chromia samples, it was concluded that dichromate bands at 246, 281, 322 and 454 nm are systematically shifted to the blue region as compared to chromate ones at

268, 294, 370 and 476 nm. Multipeak deconvolution was consistent with 36% population of chromate and 64% dichromate for chromia–silica samples with 0.2 wt% of Cr loading. Hydrated CrO_x/SiO_2 samples with Cr in 6+ oxidation state and 0.2 wt% Cr loading were found to have bands at 240 and 348 nm with a shoulder at 429 nm [30], which were ascribed to dichromate species. It is worth noting that the chromate band around 460 nm should be ascribed to the symmetry forbidden transition ($1t_1 \rightarrow 2e$). The distortion of tetrahedral symmetry upon deposition on support material can be expected to greatly influence the intensity of the corresponding band and may become a source of confusion.

Although the presence of chromate species in our samples is likely, consideration of the Raman and UV–Vis spectra in Figs. 1 and 2 combined with the analysis of literature data favors assignment of the dominant chromia species in CrO_x/SiO_2xr/PE-MCM-41, CrO_x/SiO_2xr, CrO_x/SiO_2xr/Cab–O–Sil samples to dichromates. The Raman spectrum of CrO_x/Cab–O–Sil sample was quite similar to that of crystalline Cr_2O_3 [29]. For CrO_x/PE-MCM-41, the band at 898 cm^{-1} can be attributed to di-and polychromates. The band at 554 cm^{-1} on the same sample can be tentatively ascribed to Cr^{3+} species. Although Raman and UV–Vis spectroscopies seem to be inconclusive with regard to the dispersity of Cr^{3+} species, the formation of Cr^{3+} species resistant to oxidation treatment usually occurs at high chromia loading and implies the formation of relatively large clusters of Cr_2O_3 [9].

The degree of catalyst hydration is among the main parameters that govern the nature of supported chromia species. Following the work by Hardcastle and Wachs [29], Kim et al. [3] argued that dehydration of the catalysts, which takes place under the reaction conditions, leads to the conversion of dimers, trimers and polymers of chromia oxide on silica to highly distorted, isolated monochromate species. As for dehydrogenation reaction, the dehydration of the catalyst is also accompanied by reduction of Cr^{6+} species into Cr^{3+}. Though little is known about the actual structure of the active site, the presence of 2 coordinative vacancies was established by Rossi et al. [12] through adsorption of NO.

The current catalysts were further characterized by temperature programmed reduction in hydrogen. As seen from Fig. 3, all in-situ calcined catalysts exhibited peaks in the 435–447 °C region. Ellison et al. [33] approximated the experimental H_2-TPR data with 4 overlapping peaks of Gaussian shape assigned to different chromia species. It was concluded that in comparison to chromates, dichromates required higher temperatures for the reduction, whereas lower temperature was required for the reduction of bulk CrO_3. Based on the results Cavani et al. [15], Liu et al. [34] alternatively suggested that the variation in the

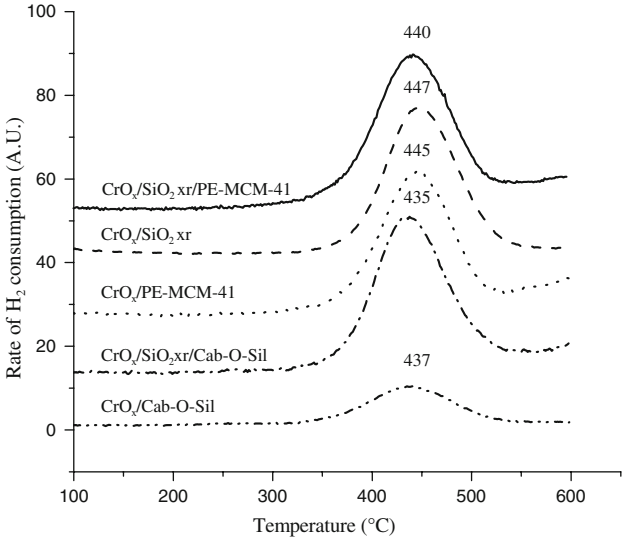

Fig. 3 TPR profile of the catalysts after their preliminary in-situ oxidation

position of TPR peak might originate from chromia species with different chromia–support interactions. There is a general consensus with regard to the overall stoichiometry of the reduction process [35]. With chromium in 6+ oxidation state, the amount of hydrogen consumed corresponds to its reduction to Cr^{3+}.

The H/Cr ratios observed for the current catalysts are summarized in Table 1. Within the margin of experimental errors, the H/Cr ratios for CrO_x/SiO_2xr/PE-MCM-41, CrO_x/SiO_2xr, CrO_x/SiO_2xr/Cab–O–Sil catalysts are close to 3. For the samples whose preparation involved a sol–gel step, the TRP results imply that before the reduction step, all chromium ions were exclusively in the 6+ oxidation state. The data also suggest that all chromium ions are available for the reaction with hydrogen. The observed H/Cr ratios, however, are lower for the samples prepared by simple impregnation of PE-MCM-41 and Cab–O–Sil silica with chromium nitrate. The most likely explanation is the presence of clusters of Cr_2O_3. As observed by McDaniel [36], such particles are stable against oxidation at high temperatures and therefore cannot participate in the following reduction with hydrogen, thus diminishing the H/Cr ratios. The presence of the relatively strong Raman bands at 551 cm^{-1} for CrO_x/Cab–O–Sil and at 554 cm^{-1} for CrO_x/PE-MCM-41 can be considered as a direct evidence of the presence of Cr^{3+} species [9] that is in line with the TPR data.

The pore size distributions of the catalysts before and after non-oxidative dehydrogenation of propane are shown in Fig. 4. Though, as shown below, the reduction in the surface area of some samples cannot be ignored, the reaction has little effect on pore size distributions. CrO_x/SiO_2xr, CrO_x/PE-MCM-41, CrO_x/Cab–O–Sil samples

Table 1 Characterization of the catalysts by H_2-TPR. The number of hydrogen atoms consumed during reduction of pre-oxidized catalysts per chromium atom in the samples

Catalyst	H/Cr ratio
$CrO_x/SiO_2xr/PE-MCM-41$	3.2
CrO_x/SiO_2xr	2.9
$CrO_x/PE-MCM-41$	2.5
$CrO_x/SiO_2xr/Cab–O–Sil$	3.0
$CrO_x/Cab–O–Sil$	0.9

possess distinctly different pore size distribution patterns. As seen in Fig. 3, CrO_x/SiO_2xr sample is mostly microporous with pores less than 4 nm. The pore size distribution of $CrO_x/PE-MCM-41$ exhibits a distinct maximum at ca. 9 nm, whereas a maximum for $CrO_x/Cab–O–Sil$ lies at 30 nm. The formation of a gel inside the pores followed by its drying and calcination may alter the pore size distribution of the original materials. As depicted in Scheme 1, three possible situations may be anticipated. In situation A, the pore sizes of preformed material are small and the gel-support interaction is strong. As drying of the gel leads to its shrinkage to a considerable degree, the dried gel would spread over the surface of the pores. If pores in a preformed support material are large and interaction between the surface of the support and the gel is weak, the formation of a xerogel similar to that formed in the absence of support is likely (case C). It should be noted also that small pores alone (regardless of the degree of gel/support interaction) can influence the structure of the forming silica layer as the formation of pores typical for pure xerogel will be suppressed. There should be a case intermediate to A and C, which is designated B in Scheme 1.

Comparison of pore size distributions for $CrO_x/SiO_2xr/PE-MCM-41$ and $CrO_x/PE-MCM-41$ shown in Fig. 3 reveals their close similarity. Moreover, the maximum for $CrO_x/SiO_2xr/PE-MCM-41$ lies at ca. 8 nm, slightly lower than the observed for $CrO_x/PE-MCM-41$. As direct HRTEM analysis was inconclusive due to low contrast of silica, and disordered pore structure, the pore size distribution measurements strongly support case A as the most suitable in describing the formation of $CrO_x/SiO_2xr/PE-MCM-41$ sample.

The pore size distribution of $CrO_x/SiO_2xr/Cab–O–Sil$ was quite broad with 2 humps at ca. 4 and 30 nm. As the hump at 30 nm is reminiscent of $CrO_x/Cab–O–Sil$ sample, the pore size distribution data favor their assignment to case B of Scheme 1, in which a layer of xerogel on the silica surfacea as well as xerogel nanoparticles form.

The catalytic activities of the prepared catalysts in non-oxidative dehydrogenation of propane are presented in Fig. 5. A blank experiment with an empty reactor gave, under otherwise the same conditions, much lower values of around 1% conversion. With the same loadings of chromium, and the same total catalyst weight, the high surface area, mesoporous $CrO_x/SiO_2xr/PE-MCM-41$ showed the

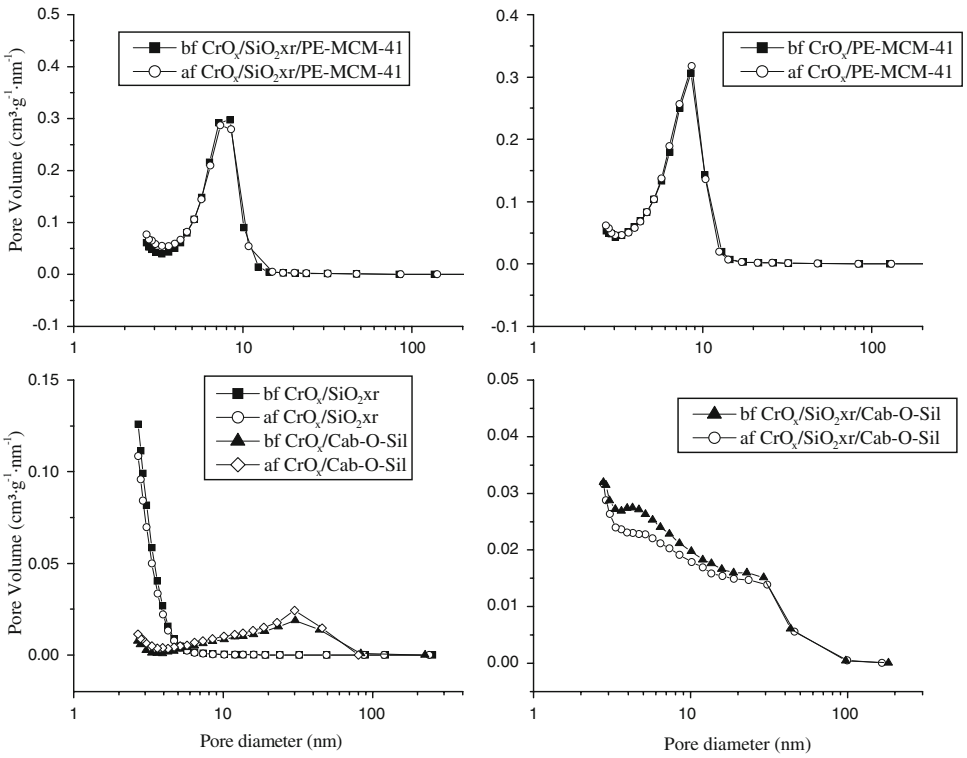

Fig. 4 Pore size distributions in granulated catalysts before and after the reaction

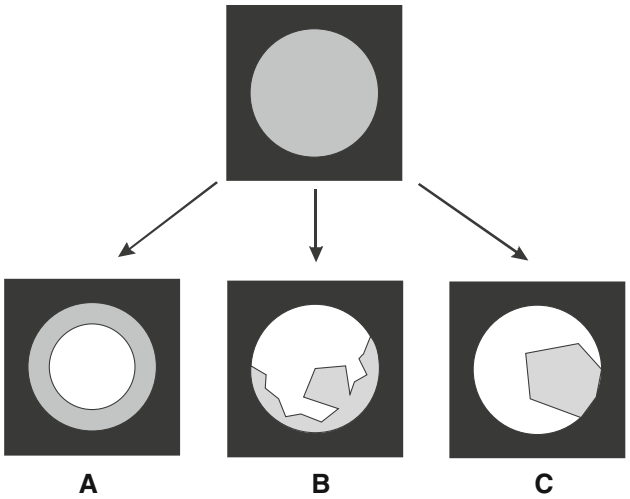

Scheme 1 Idealized picture of three possible fates of the chromia-doped gel formed inside of the porous structure upon the sample drying and calcination. Black is a preformed silica support such as PE-MCM-41 or Cab–O–Sil, grey is a chromia-doped gel and xerogel

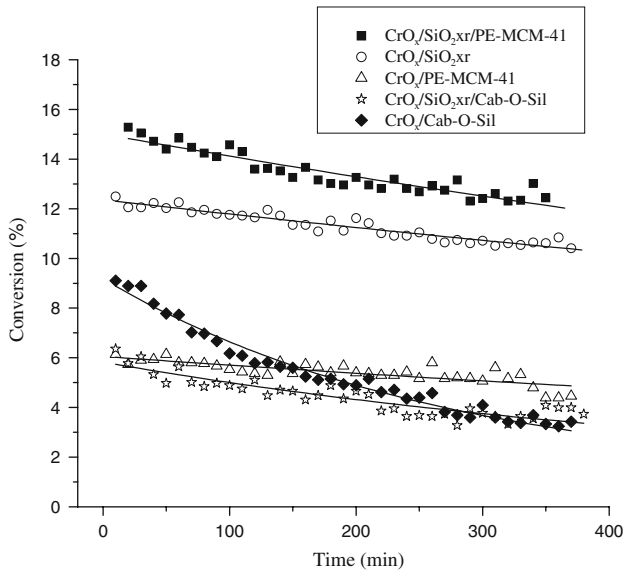

Fig. 5 Conversion of propane vs. time on stream over different catalysts

highest activity. The hard, dense and easy-to-prepare microporous CrO_x/SiO_2xr demonstrated good conversion of propane. CrO_x/SiO_2xr/Cab–O–Sil, CrO_x/PE-MCM-41, CrO_x/Cab–O–Sil catalysts demonstrated much lower activities in comparison with the two most active samples.

Non-oxidative dehydrogenation of light alkanes over chromia–silica catalysts was studied in considerable detail earlier [3, 11, 12]. The study by Rossi et al. [12] of propane dehydrogenation over chromia–silica catalysts demonstrated that regardless of the initial oxidation state of chromium, +3 or +2, the activity of the catalysts were the same after 5 min of time on stream. Moreover, prior reduction of the catalyst by H_2 or CO was found unnecessary, as activity of calcined catalysts, with chromium in 6+ oxidation state, were identical to the reduced ones just after 5 min on stream. It was concluded that under non-oxidative dehydrogenation conditions, a fast reduction or oxidation of chromium species takes place to produce mononuclear Cr^{3+} as the active sites.

The UV–Vis spectrum of the spent CrO_x/SiO_2xr/PE-MCM-41 catalyst recorded under ambient conditions is in line with the literature data as conversion of Cr^{6+} into Cr^{3+} species is obvious due to the appearance of a broad band at ca. 600 nm. Absorption in the region below 500 nm may originate from overlapping bands belonging to Cr^{3+} (295, 465 nm [31]) with absorption of Cr^{6+} species. Quasi in-situ XPS experiments[1] during non-oxidative dehydrogenation of ethane over chromia–silica catalysts have been carried out recently in our laboratory [Rao TVM, Sayari A unpublished data]. The results strongly support the notion of conversion Cr^{6+} into Cr^{3+}.

The deactivation of catalysts occurred in all cases. The deactivation of CrO_x/SiO_2xr/PE-MCM-41, however, slowed down upon reaction progress, whereas the deactivation of CrO_x/SiO_2xr was fairly slow right from the reaction start. Interestingly, opposite to CrO_x/SiO_2xr/PE-MCM-41 and CrO_x/SiO_2xr containing highly dispersed chromium species on high surface area support, deactivation of Cr_2O_3 crystallites on relatively low surface are Cab–O–Sil was much faster. Deactivation in the case of CrO_x/SiO_2xr/Cab–O–Sil containing highly dispersed chromia on low surface area Cab–O–Sil was significant in terms of relative values. In most cases, catalyst deactivation was accompanied by an increase in the selectivity to propane from 74 to 85% for CrO_x/SiO_2xr/PE-MCM-41, from 75 to 77% for CrO_x/SiO_2xr, from 87 to 96% for CrO_x/SiO_2xr/Cab–O–Sil, and from 84 to 96% for CrO_x/Cab–O–Sil. The selectivity for CrO_x/PE-MCM-41 remained roughly the same and close to 86%.

The CrO_x/SiO_2xr/PE-MCM-41 and CrO_x/PE-MCM-41 catalysts possess similar surface areas but very different catalytic activities. The most likely explanation to this phenomenon is the much higher dispersity of chromia species in the case of CrO_x/SiO_2xr/PE-MCM-41 than in CrO_x/PE-MCM-41. Indeed, as it was revealed by Raman spectroscopy the band at 554 cm^{-1} observed in CrO_x/PE-MCM-41 is consistent with the presence of Cr^{3+} species resistant to oxidation that in turn is characteristic of relatively large clusters of Cr_2O_3. In addition, CrO_x/SiO_2xr/PE-MCM-41 does not exhibit a Raman band around 554 cm^{-1}, though the 898 cm^{-1} band characteristic of dichromate is

[1] The dehydrogenation reaction was conducted in a separate catalytic reactor attached to the surface measurement instrument, then the catalyst was moved to the analysis chamber without exposure to air.

clearly present. This implies that as compared to CrO_x/PE-MCM-41, utilization of sol–gel step helps spread chromia species, whereas for CrO_x/PE-MCM-41 the lack of anchoring sites leads to bigger chromia clusters. Larger chromia clusters would naturally have a smaller number of surface sites available for the catalytic reaction and can be expected to demonstrate lower catalytic activity than if presented in more dispersed chromate and dichromate forms.

An attempt was made to find correlations between the catalyst activity/stability and other properties of the catalysts. A plot of catalyst activity at the beginning and at the end of the reaction vs. the corresponding surface area of the catalysts is shown in Fig. 6. As zero catalyst surface area would mean dehydrogenation through non-catalytic process only, all correlation lines pass through this value, i.e. ca. 1%. Comparison of the catalysts whose preparation involved spreading chromia species through a sol–gel step, namely CrO_x/SiO_2xr/PE-MCM-41, CrO_x/SiO_2xr, and CrO_x/SiO_2xr/Cab–O–Sil revealed that their initial activities are directly proportional to their total surface areas. The other two catalysts, CrO_x/PE-MCM-41, CrO_x/Cab–O–Sil, prepared by impregnation of preformed silica supports by the chromium salt fell out of the correlation line. Correlation of the activity vs. surface area for CrO_x/SiO_2xr/PE-MCM-41, CrO_x/SiO_2xr, and CrO_x/SiO_2xr/Cab–O–Sil samples at the reaction completion (6 h on stream) is less compelling as microporous CrO_x/SiO_2xr seems to fall out of the line. It should be noted also that even for similarly prepared catalysts, differences in activities cannot be directly related to their pore structure. Indeed, CrO_x/SiO_2xr possesses fairly small pores but greatly surpasses in activity CrO_x/SiO_2xr/Cab–O–Sil sample which exhibits a significant portion of large pores.

Comparison of catalytic activity and TPR data for CrO_x/SiO_2xr/PE-MCM-41, CrO_x/SiO_2xr, and CrO_x/SiO_2xr/Cab–O–Sil sample leads to an interesting observation. According to TPR data all chromium atoms in these samples are available to reduction from Cr^{6+} to Cr^{3+}. However, the initial turnover frequency calculated with respect to the total number of chromium atoms change from $15 \cdot 10^3$ s^{-1} $atom^{-1}$ for CrO_x/SiO_2xr/PE-MCM-41, to $12.4 \cdot 10^3$ s^{-1} $atom^{-1}$ for CrO_x/SiO_2xr and $6 \cdot 10^3$ s^{-1} $atom^{-1}$ for CrO_x/SiO_2xr/Cab–O–Sil. In an earlier investigation of propane dehydrogenation over chromia–silica catalysts, Rossi et al. [12] found that the turn over frequencies of catalysts prepared by a simple impregnation method were independent of chromium loading, implying the occurrence of similar structure of the active sites in all catalysts. The sol–gel preparation approach used in this work produced a different outcome. Indeed, the turnover frequencies were found to vary strongly among similarly prepared catalysts. One of the possible explanations to this phenomenon may lie in the variation of a structure of active sites—a hypothesis, which requires further research for its justification.

Deactivation of the catalysts due to coke formation is a major problem in the production of olefins via non-oxidative dehydrogenation route. The deactivation rates were quantitatively assessed by fitting experimental data with typical exponential decay function [12]:

$$a(t) = a_{nc} + a_0 e^{-kt},$$

where t is the time on stream, k is the rate of deactivation, min^{-1}, a(t) is the total conversion of propane at time t, a_{nc} is the conversion of propane with no catalyst, and a_0 is the catalytic conversion at the beginning of the reaction. The best fits shown in Fig. 5 by solid lines produce generally adequate representation of experimental data. The obtained deactivation rates, k, were plotted vs surface areas in Fig. 7. At the same chromium loading, the experimental data seem to indicate that catalysts with large surface areas are less prone for deactivation.

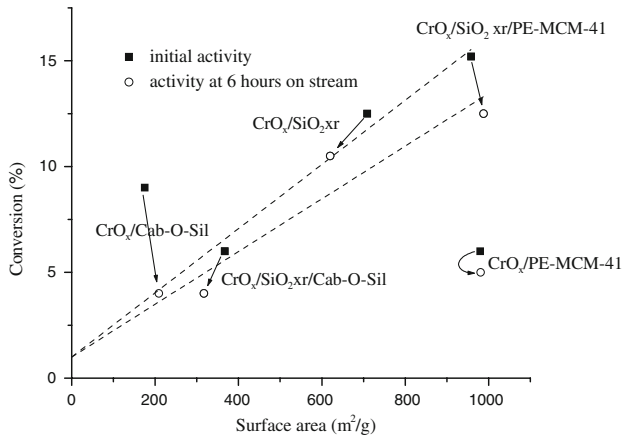

Fig. 6 Conversion of propane at the beginning and the end (6 h on stream) of the reaction vs. surface areas of the catalysts

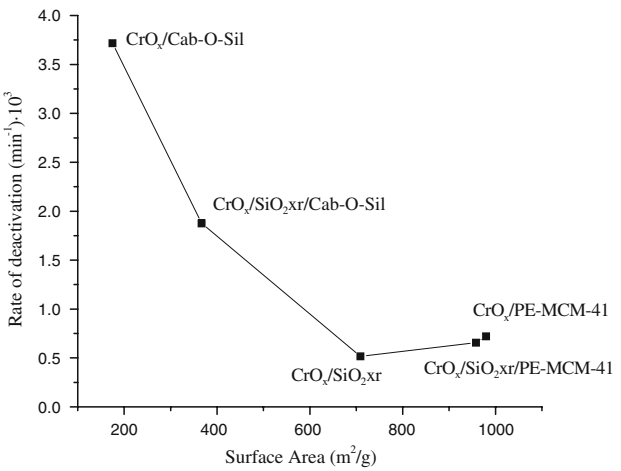

Fig. 7 Deactivation rate vs. surface areas of the catalysts

4 Conclusions

The sol–gel assisted deposition of chromia species on a preformed silica support is a versatile synthetic route allowing the formation of catalysts with desired pore structures and chromia species in a highly dispersed state. The activity of chromia–silica catalysts prepared through the sol–gel assisted procedure was found to be surface area dependent and for the best samples greatly surpassed activity of catalysts prepared by impregnation. For samples whose preparation involved a sol–gel step, the catalytic activity was found to be proportional to the catalyst surface area, whereas among all the samples tested, an increase in the surface generally entailed higher catalyst stability.

Acknowledgments We thank the Natural Science and Engineering Council of Canada (NSERC) for financial support. A.S. is the Government of Canada Research Chair in *Catalysis by Nanostructured Materials* (2001–2008).

References

1. Clark JH, Kybett AP, Landon P, Macquarrie DJ, Martin K (1989) J Chem Soc Chem Commun 1355
2. Parlitz B, Hanke W, Fricke R, Richter M, Roost U, Ohlmann G (1985) J Catal 94:24
3. Kim DS, Tatibouet J-M, Wachs IE (1992) J Catal 136:209
4. Weckhuysen BM, Schoonheydt RA (1999) Catal Today 51:215
5. Chatterjee S, Greene HL (1991) J Catal 130:76
6. Bhasin MM, McCain JH, Vora BV, Imai T, Pujado PR (2001) Appl Catal A Gen 221:397
7. Sanfilippo D, Miracca I (2006) Catal Today 111:133
8. Brazdil JF (2006) Top Catal 38:289
9. Weckhuysen BM, Wachs IE, Schoonheydt RA (1996) Chem Rev 96:3327
10. Weckhuysen BM, Schoonheydt RA (1999) Catal Today 51:223
11. Lugo HJ, Lunsford JH (1985) J Catal 91:155
12. De Rossi S, Ferraris G, Fremiotti S, Garrone E, Ghiotti G, Campa MC, Indovina V (1994) J Catal 148:36
13. De Rossi S, Ferraris G, Fremiotti S, Cimino A, Indovina V (1992) Appl Catal A Gen 81:113
14. Hakuli A, Kytokivi A, Krause AOI, Suntola T (1996) J Catal 161:393
15. Cavani F, Koutyrev M, Trifiro F, Bartolini A, Ghusletti D, Iezzi R, Santucci A, Del Piero G (1996) J Catal 158:236
16. Ashmawy FM (1980) J Chem Soc Faraday Trans 76:2096
17. Weckhuysen BW, Bensalem A, Schoonheydt RA (1998) J Chem Soc Faraday Trans 94:2011
18. Sayari A (2004) Mesoporous silica and silica–organic hybrids. In: Atwood JL, Steed JW (eds) Encyclopedia of supramolecular chemistry. Marcel Dekker, p 852
19. Sayari A, Kruk M, Jaroniec M, Moudrakovski IL (1998) Adv Mater 10:1376
20. Sayari A, Yang Y, Kruk M, Jaroniec M (1999) J Phys Chem B 103:3651
21. Sayari A (2000) Angew Chem Int Ed 39:2920
22. Serna-Guerrero R, Sayari A (2007) Environ Sci Tech 41:4761
23. Kruk M, Jaroniec M, Sayari A (1997) Langmuir 13:6267
24. Dietz WA (1967) J Gas Chromatogr 5:68
25. Deo G, Wachs IE (1991) J Phys Chem 95:5889
26. Ramani NC, Sullivan DL, Ekerdt JG, Jehng J-M, Wachs IE (1998) J Catal 176:143
27. Vuurman MA, Wachs IE, Stufkens SJ, Oskam A (1993) J Mol Catal 80:209
28. Vuurman MA, Stufkens DJ, Oskam A, Moulijn JA, Kapteijn F (1990) J Mol Catal 60:83
29. Hardcastle FD, Wachs IE (1988) J Mol Catal 46:173
30. Weckhuysen BM, Schoonheydt RA, Jehng J-M, Wachs IE, Cho SJ, Ryoo R, Kljlstra S, Poels E (1995) J Chem Soc Faraday Trans 91:3245
31. Weckhuysen BM, De Ridder LM, Schoonheydt RA (1993) J Phys Chem 97:4756
32. Weckhuysen BM, Verberckmoes AA, Buttiens AL, Schoonheydt RA (1994) J Phys Chem 98:579
33. Ellison A, Overton TL, Bencze L (1993) J Chem Soc Faraday Trans 89:843
34. Liu L, Li H, Zhang Y (2007) Catal Commun 8:565
35. Gaspar AB, Brito JLF, Dieguez LC (2003) J Mol Catal A Chem 203:251
36. McDaniel MP (1982) J Catal 76:37